CrossMark

Effect of Pr addition on properties and Sn whisker growth of Sn–0.3Ag–0.7Cu low-Ag solder for electronic packaging

Jie Wu[1] · Songbai Xue[1] · Jingwen Wang[1] · Jianxin Wang[2] · Shuang Liu[1]

Abstract In this study, trace amount of rare earth Pr was added into Sn–0.3Ag–0.7Cu low-Ag solder to enhance properties of solders. Experimental results indicated that optimal amount of Pr addition (~0.06 wt%) can improve properties of wettability, shear force and ductility of Sn–0.3Ag–0.7Cu low-Ag solder. This is because that solder with optimal Pr addition not only had a refined microstructure but also owned a regular and thin interfacial IMC layer after soldering on Cu substrate. Meanwhile, we have explained the change of morphology and thickness of interfacial IMC layer after Pr addition based on Kim and Tu's kinetic model of interfacial IMC growth. However, it was found excessive Pr addition led to the formation of $PrSn_3$ phase, which was easy to be oxidized and became a great deterioration on the properties referred above. Besides, the fracture mode of solder joint also gradually changed from ductile fracture to cleavage fracture. Moreover, this oxidized $PrSn_3$ became the birthplace of Sn whisker since it provided abundant supply of Sn sources and compressive stress for Sn whisker growth. By the in-situ observation of Sn whisker growth in 0.5 wt% Pr-doped solder joint, we obtained that the incubation period of Sn whisker is very short and its growth rate may have a great decrease with time extending. Besides, it was found after 1 day at room temperature, spindly and rod-like Sn whiskers also grew in 0.5 wt% Pr-doped solder joint besides dot-shaped Sn whisker that grew in 0.5 wt% Pr-doped solder matrix. We suggest this may be related with the extra compressive stress provided by interfacial IMC layer growth in 0.5 wt% Pr-doped solder joint.

1 Introduction

Under the high pressure of environmental directives like WEEE and RoHS, utilization of conventional Sn–Pb solders in microelectronics has been extensively limited due to the existence of toxic and not environment-friendly element of Pb [1–3]. Therefore, massive investigations on synthesizing novel lead-free solders were underway to seek for suitable substitutions for Sn–Pb solders. Among all the alternatives including Sn–Zn, Sn–Ag, Sn–Cu binary systems and Sn–Zn–Bi, Sn–Ag–Cu, Sn–Cu–Ni ternary systems, Sn–Ag–Cu system has been widely considered as the most promising and attractive candidate for its comparatively favorable wettability and mechanical properties [4–6]. In recent years, a variety of eutectic/near-eutectic Sn–Ag–Cu solder alloys have been recommended for practical applications in different countries, such as Sn–3.8Ag–0.7Cu in EU, Sn–3.9Ag–0.6Cu in US and Sn–3.0Ag–0.5Cu in Japan [7, 8]. However, high price of valuable metal (Ag) that will raise production cost is a notable weak point, which may hinder the large-scale application of Sn–Ag–Cu high-Ag solders. Therefore, study and application of Sn–Ag–Cu low-Ag solder seems pretty essential. It was found that when compared with high-Ag solder joint, Sn–Ag–Cu low-Ag solder joint free of bulk Ag_3Sn IMCs exhibits a higher resistance to drop failure. However, when compared with tradition Sn–Pb solders, these Sn–Ag–Cu low-Ag solders still have lots

✉ Songbai Xue
  xuesb@nuaa.edu.cn

[1] College of Materials Science and Technology, Nanjing University of Aeronautics and Astronautics, Nanjing 210016, People's Republic of China

[2] Jiangsu Provincial Key Laboratory of Advanced Welding Technology, Jiangsu University of Science and Technology, Zhenjiang 212003, People's Republic of China

of shortcomings, such as a bit too high melting temperature, relatively poor wettability and excessive interfacial compound growth [4, 9]. Therefore, in order to modify these properties of solder joints, various fourth elements (e.g., Zn, Ga, In, Ni, Sb) were selected to be added into Sn–Ag–Cu low-Ag solders [10–13]. Unfortunately, their optimizations were not that comprehensive. For instance, although adding elemental In and Ga lowered down the melting point and improved the wettability of corresponding solders, its contribution to mechanical properties was somewhat unsatisfactory when compared with alloys with Zn and Ni addition. But, the addition of alloys like Zn may lead to easy oxidation of molten solder, which can worsen the wettability or bond reliability. Nowadays, with the extensive prevalence of nanotechnology, low-Ag solder with nanoparticle addition is gradually arousing global research interest due to a mount of specific properties that nanoparticles own [14–16]. However, since nanoparticles are easy to be oxidized and prone to have agglomeration, it became difficult to make them distribute uniformly in the solder without agglomeration. So, preparations of low-Ag solders with nanoparticle additions are complex, which also increase the production cost. By contrast, the surface-active rare earth (RE) elements (e.g., La [17], Ce [18], Pr [8], Nd [2, 4], Eu [19], Yb [5]), known as "vitamins" in alloys, have attracted researchers' attention. It has been demonstrated that RE addition in solders played a positive role in both microstructure amelioration and property improvement (e.g., wettability, pull and shear strength, reliability). However, it was also found that excessive RE addition led to the formation of RE-Sn phase, which was easy to be oxidized and then became the birthplace of Sn whiskers [6, 20].

Our previous study showed that the wettability and shear force of Sn–0.3Ag–0.7Cu low-Ag solder were apparently improved by optimal Nd addition [2]. This new finding prompts us to study the influence of trace amount of Pr addition on the microstructure and relative properties of Sn–0.3Ag–0.7Cu solder due to the assumption of a variety of similar physical–chemical qualities between Pr and Nd according to their specific position on the periodic table. Therefore, various contents of Pr (0–0.5 wt%) was added into Sn–0.3Ag–0.7Cu low-Ag solder. Besides, due to the possible generation of Sn-Pr

phase, in-situ observation was taken to get some findings of Sn whisker growth.

2 Experimental procedure

2.1 Alloy design and preparation

In order to synthesize Sn0.3Ag0.7Cu alloy, raw materials including pure metals of Sn, Ag, and Cu all with purity of 99.95 wt% were melted at $900 \pm 10\,°C$ in a vacuum furnace. Since RE Pr is prone to be oxidized if fused barely into Sn0.3Ag0.7Cu alloy, master alloy ingots of Sn–10Pr should be prepared first—that includes, fusing Sn and Pr with purity of 99.5 wt% at $900\,°C$ for about 15 min under vacuum atmosphere (10^{-3} torr). Subsequently, master alloy of Sn–10Pr was put into molten Sn0.3Ag0.7Cu alloy at $550 \pm 1\,°C$ for about 40 min with a stainless steel rod stirring the molten alloy every 1 min to homogenize the molten alloy. RE Pr-containing Sn0.3Ag0.7Cu alloy could be obtained then. Afterwards, the molten alloy was chilled to cast in air and cut into small bars with about 40 mm in length. Table 1 lists the investigated Pr-containing Sn–0.3Ag–0.7Cu solders with seven kinds of compositions (0–0.5 wt%).

2.2 Wetting property test

The wetting balance method [21] was applied to measure the wettability of Sn–0.3Ag–0.7Cu–xPr solders (x=0-0.5 wt%) using SAT-5100 Solder Checker. The experimental parameters of immersion depth, speed and time were set as 2 mm, 4 mm/s and 10 s, respectively. The test Cu foils (30mm×5mm×30 mm) coating with water-soluble flux were firstly ultrasonic cleaned in acetone for 3 min and then cleaned in ethanol and dried before practical test. To know how temperature and gas type affect the wettability of solders, the experiments were carried out at different temperatures (235, 245, 255 and 265 °C) and in different gas type (air and N$_2$ atmosphere).

2.3 XRD phase analysis and microstructure observation

First, phase identification approached by X-ray diffraction (XRD) with Cu K$_\alpha$ radiation at 40 kV (40 mA) and with a scan speed of 4°/min was conducted to ascertain the basic

Table 1 Chemical compositions of solder alloys

Serial number	a	b	c	d	e	f	g
The content of Pr/wt%	0	0.015	0.03	0.06	0.12	0.25	0.5
Original alloy	Sn–0.3Ag–0.7Cu						
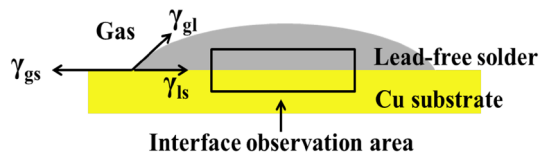
Fig. 1 Schematic diagram of interface observation area

Fig. 2 Schematic illustration of shear force test

phases in the Sn–0.3Ag–0.7Cu–xPr (x = 0–0.5 wt%) solder. It should be mentioned that XRD has a limitation to detect phases below a certain content. Therefore, further phase observation with the assistance of OM, SEM and EDS should be conducted to know the accurate structure evolution. So, it's essential to study the change of solder microstructure after Pr addition. Firstly, the specimens sliced from the same place of each casting were carefully polished with 0.3 μm Al_2O_3 powder and then they were etched by a solution of 4% HNO_3-alcohol for 3–5 s. With assistance of optical microscope (OM) and SEM, microstructure observation was realized. Besides, typical interfacial microstructure of Sn–0.3Ag–0.7Cu–xPr solder joint (x = 0, 0.06 and 0.5 wt%) were also studied. These solder joints were obtained at 265 °C for about 80 s in an electrical resistance furnace. Then, the solder joint was crossed-sectioned to observe its interfacial microstructure, as shown in Fig. 1. Finally, Image J software was used to calculate the average thickness of interfacial IMC layer based on the following equation:

$$\bar{x} = A_i/l_i \tag{1}$$

where $\bar{x}$ represents the average thickness of interfacial IMC layer, A_i is the total area of the measured interfacial IMC layer and l_i stands for the length of this IMC layer. Besides, By in-situ observation of Sn whisker growth in 0.5 wt% Pr-doped solder joint, some findings were also obtained.

2.4 Mechanical property test

Before shear test beginning, ceramic resistors (0805, 2 mm × 1.2 mm × 0.5 mm) were manually-soldered on Cu foils attached on the printed circuit board (PCB) using investigated solders with help of water-soluble flux at about 265 °C. Afterwards, these specimens were annealed at 100 °C for 2 h to reduce the residual stress induced during specimen preparation. With the guidance of the Japan industry standard JIS Z3198-7 [22], shear test was carried out using STR-1000 Micro-joint strength tester, as shown in Fig. 2. To understand the effect of Pr addition on shear force, typical shear fracture surfaces were selected to be observed with the help of scanning electron microscope (SEM) equipped with energy dispersive X-ray spectroscopy (EDS). Meanwhile, their failure mechanisms were analyzed as well.
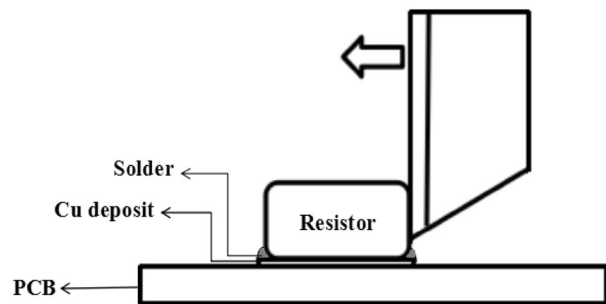
3 Results and discussion

3.1 Wettability

Wettability describes the tendency of molten solder wetting and spreading on solid substrate, which is a prerequisite to obtain reliable solder joints. It can be evaluated by wetting balance method [21]. Generally, a trend of decrease in wetting time along with increase in wetting force under the same condition signifies a promoted wetting performance. Figures 3 and 4 illustrate the wetting performance of Sn–0.3Ag–0.7Cu–xPr solders (x = 0–0.5 wt%) in air and N_2 atmosphere and with soldering temperature gradually elevating from 235 to 265 °C. Clearly, whether in air or in N_2 atmosphere at a certain temperature, with the increase of Pr addition from 0 to 0.5 wt%, the wetting time rapidly decreased first and then had a slow increase. However, the wetting force had a completely opposite trend. This signifies that with the increase of Pr addition, the wettability of Pr-doped Sn–0.3Ag–0.7Cu solder was evidently improved first and then had a gradual deterioration. Therefore, there exists an optimal content of Pr addition that can make the wettability of solder reach the best. Here, the optimal content of Pr addition is about 0.06 wt%. This change in wettability after Pr addition is attributed to the surface-active property of Pr. When solders begins to melt, RE Pr tends to accumulate at the solder interface, which can lower the surface tension of solder (γ_{gl} in Fig. 1) and finally improves the wettability. However, RE elements are also prone to be oxidized, which may cause oxidization slags and hinder the flow of molten solders. As a result, the wettability of solders might be ruined.

Also, elevating the soldering temperature to a proper extent can better the wetting performance. As can be seen from Figs. 3 and 4, whether at air or at N_2 atmosphere, with the temperature elevating from 235 to 265 °C, the
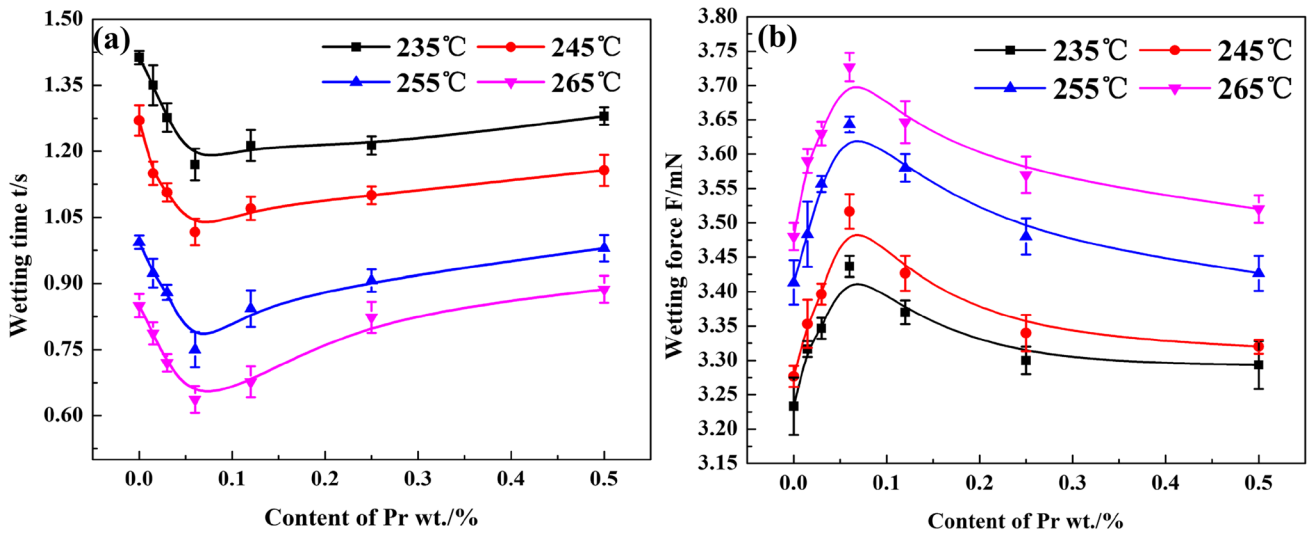
Fig. 3 Wetting performance of Sn–0.3Ag–0.7Cu–xPr solders (x = 0–0.5 wt%) in air: **a** wetting time; **b** wetting force
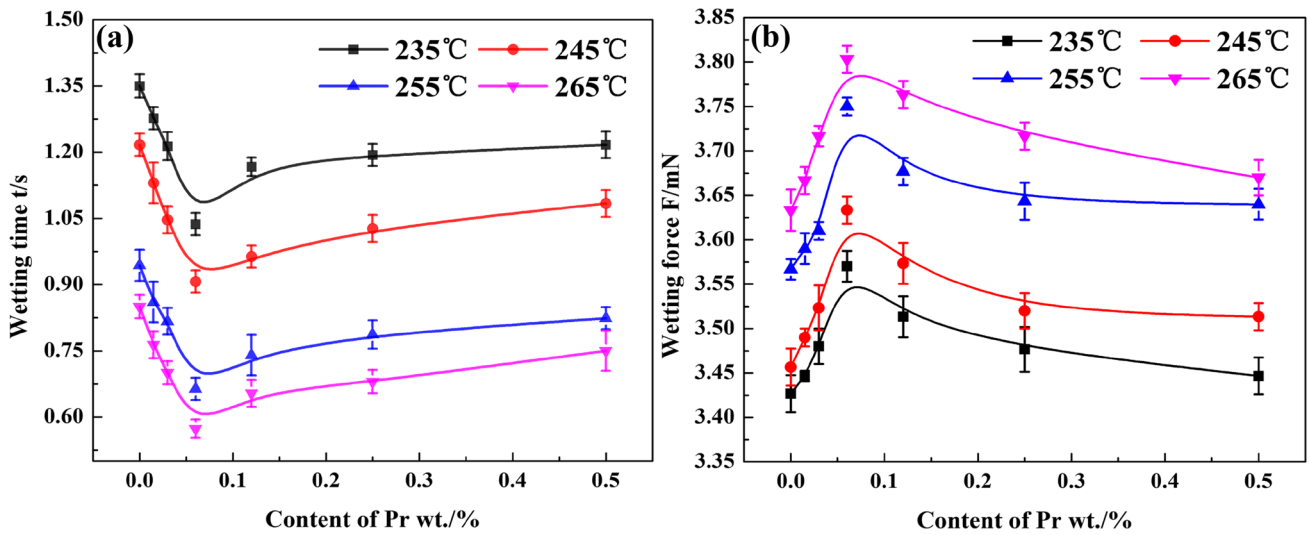

Fig. 4 Wetting performance of Sn–0.3Ag–0.7Cu–xPr solders (x = 0–0.5 wt%) in N$_2$ atmosphere: **a** wetting time; **b** wetting force

wetting time of a certain Pr-containing solder decreased and the wetting force increased simultaneously. This is mainly due to the accelerated atom diffusion at the interface when temperature elevates to a certain degree. Worthy of note was that at the temperature of 265 °C, the wetting times of Sn–0.3Ag–0.7Cu–xPr (x = 0–0.5 wt%) solders were all lower than 1 s whether in air or N$_2$ atmosphere. This was conformed with the requirements of wave-soldering in electronic industry according to the standards of IPC-J-STD-003B [23]. Therefore, the practical soldering temperature is recommended around 265 °C when Pr-modified Sn–0.3Ag–0.7Cu solder was used to fabricate solder joints in wave-soldering. However,

it should be mentioned that an increase in temperature, nominally conducing to wettability improvement, may cause RE oxidation, which in reverse hinder the wetting process. Further, the phenomenon of Cu substrate dissolution may occur if soldering temperature elevates without a base line.

Besides, Fig. 5 shows the comparative results of wetting behaviors of Sn–0.3Ag–0.7Cu–0.06Pr solder in air and in N$_2$ atmosphere over all examined temperatures. It can be seen that the wetting behaviors (wetting time and wetting force) were better in N$_2$ atmosphere than those in air. This is because that the oxidation of molten solder may become more severe in air than that in N$_2$ atmosphere.
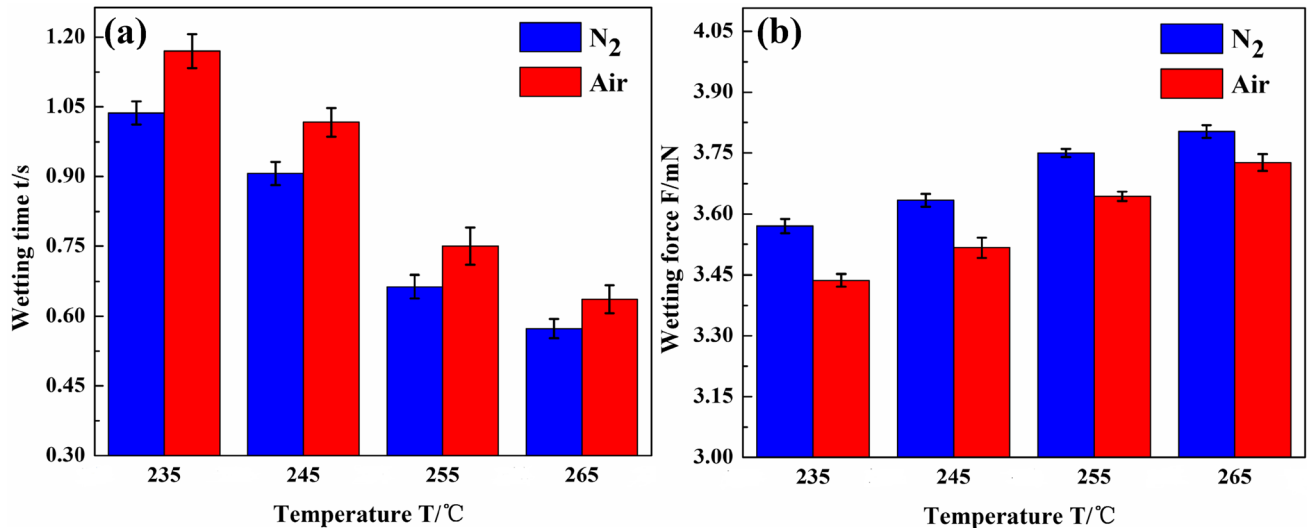
Fig. 5 Comparative results of wettability of Sn–0.3Ag–0.7Cu–0.06Pr solder in N_2 atmosphere and in air with temperature evaluating from 235 to 265 °C: **a** wetting time; **b** wetting force

3.2 XRD phase analysis

Typical XRD spectra within a wide 2θ range (20°–85°) and a narrow 2θ range (31.7°–32.4°) of Sn–0.3Ag–0.7Cu–xPr solders (x = 0–0.5 wt%) are depicted in Fig. 6. As shown in Fig. 6a, the diffraction peaks of β-Sn phase and IMCs of Ag_3Sn and Cu_6Sn_5 can be dominantly observed in all Sn-0.3Ag–0.7Cu–xPr solders, indicating that minor amount of Pr addition only affected part of reactions between Sn and Ag or Sn and Cu. Rather, the peaks of Ag_3Sn phase are of low intensity and are nor prominently seen possibly due to their low

volume fraction caused by the low Ag content in solders. One standard diffraction peak for β-Sn (101) was taken for a comparison as indicated in Fig. 6b. Clearly, after minor amount of Pr addition, an obvious decrease in the height of strongest peak of β-Sn (101) occurred, which is related to the "Sn-affinity" characteristic owned by RE Pr. It should be mentioned that XRD has a limitation to detect phases below a certain content. Therefore, further phase observation with the assistance of OM, SEM and EDS should be conducted to know the accurate structure evolution.
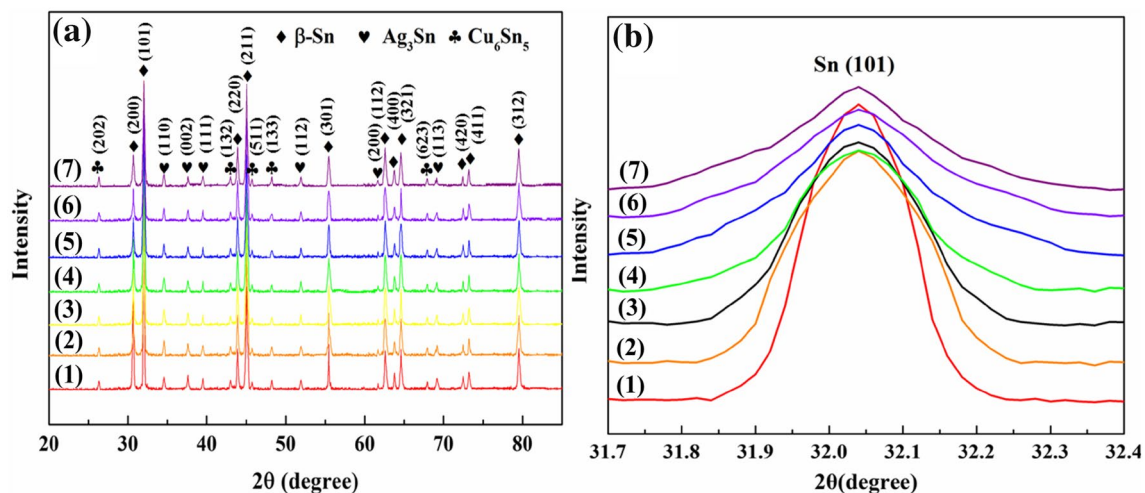

Fig. 6 XRD analysis of Sn–0.3Ag–0.7Cu–xPr solder ((*1*) x = 0, (*2*) x = 0.015, (*3*) x = 0.03, (*4*) x = 0.06, (*5*) x = 0.12, (*6*) x = 0.25, (*7*) x = 0.5 wt%): **a** a wide 2θ range of 20°–85°; **b** a narrow 2θ range of 31.7°–32.4°
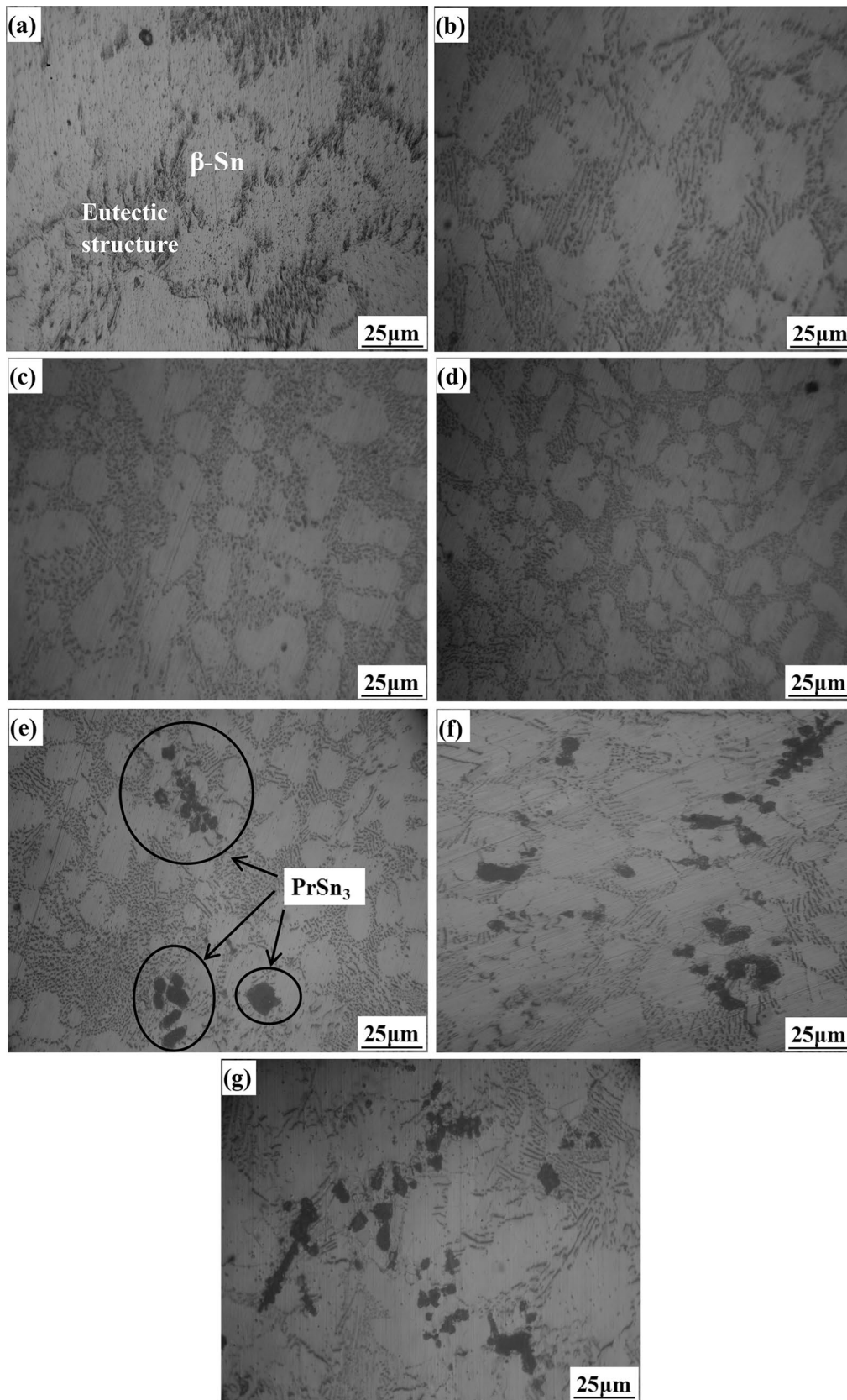
Fig. 7 Microstructure of Sn–0.3Ag–0.7Cu–xPr solders: **a** x = 0; **b** x = 0.015; **c** x = 0.03; **d** x = 0.06; **e** x = 0.12; **f** x = 0.25; **g** x = 0.5
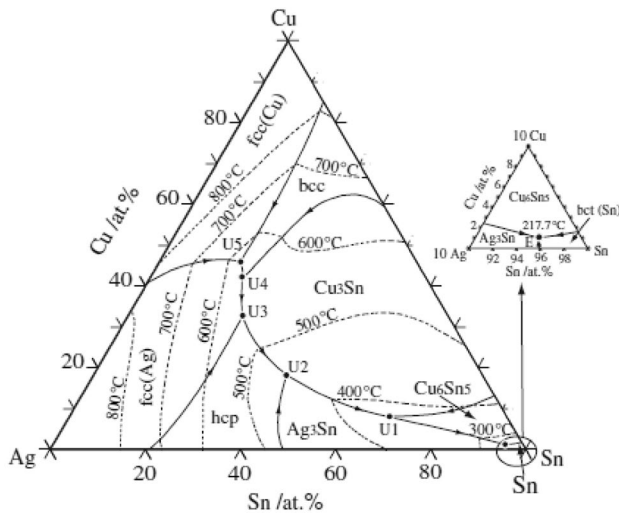
Fig. 8 Sn–Ag–Cu ternary phase diagram [26]

3.3 Microstructure evolution

3.3.1 Solder matrix

The property variations studied above are closely associated with the solder microstructure, which make it essential to fully investigate the effect of Pr addition on the microstructure of Sn–0.3Ag–0.7Cu. Figure 7 shows the optical micrographs of microstructure evolution of as-cast Sn–0.3Ag–0.7Cu–xPr solders (x = 0–0.5 wt%). As can be seen from Fig. 7a, the microstructure of original Sn–0.3Ag–0.7Cu solder consisted of light-gray dendrites and a dark-gray eutectic region. Based on the Sn–Ag–Cu ternary phase diagram (Fig. 8 [24]), it is suggested that the light-gray zone is β-Sn phase and dark-gray eutectic region was composed of β-Sn phase and $Ag_3Sn + Cu_6Sn_5$ IMCs. As shown in Fig. 7b–d, after minor amount of Pr addition (0.015–0.06 wt%), the microstructure of the solder was gradually refined and with maximum refinement
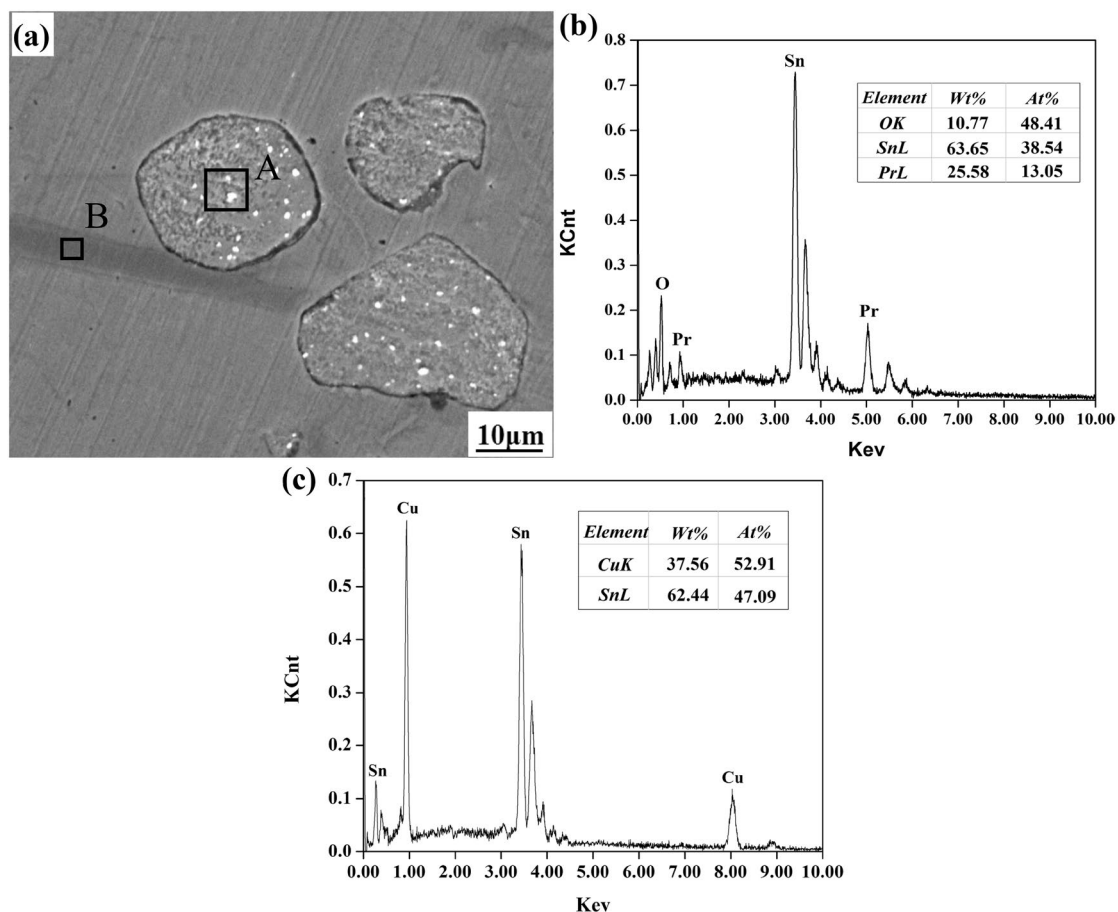

Fig. 9 The analyzed results of black phase in Sn–0.3Ag–0.7Cu–0.5Pr solder matrix after 1 day at room temperature: **a** SEM image of black phase; **b** EDS result of the area *A* in (**a**); **c** EDS result of the area *B* in (**a**)
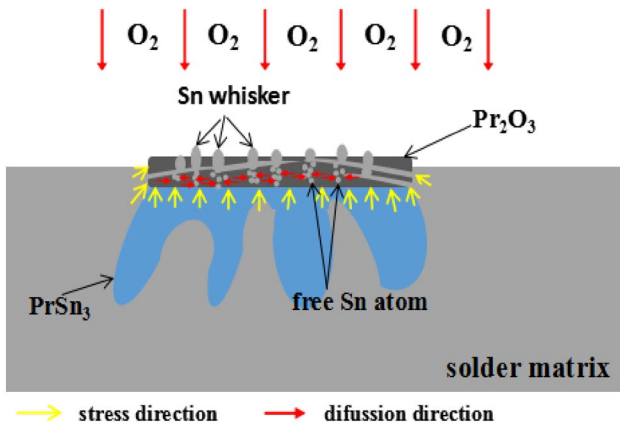
Fig. 10 Schematic illustration of the formation and development mechanism of Sn whisker

realized for the solder containing 0.06 wt% Pr. Therefore, it's the relative small area of β-Sn phase with suitable volume fraction of the eutectic colony that contributes to a good mechanical property of Sn–0.3Ag–0.7Cu–0.06Pr. Rather, with Pr addition further increasing to 0.5 wt%, the β-Sn phase gradually became large than before and eutectic region got sparse, as shown in Fig. 7e–g. This change in microstructure indicates that partial amount of Pr addition has lost its effectiveness. Besides, as can be seen from Fig. 7e–g, some black and fish-bone shaped phases also appeared in the solder matrix. To know the accurate composition of these black phases, Fig. 9 gives the magnified SEM image and EDS analyzed results of localized region containing black phases in 0.5Pr-doped solder matrix after 1 day at room temperature. Clearly, the black phase in Fig. 9a (marked with A) existing at the interface between the strip-shaped IMC (marked with B) and the
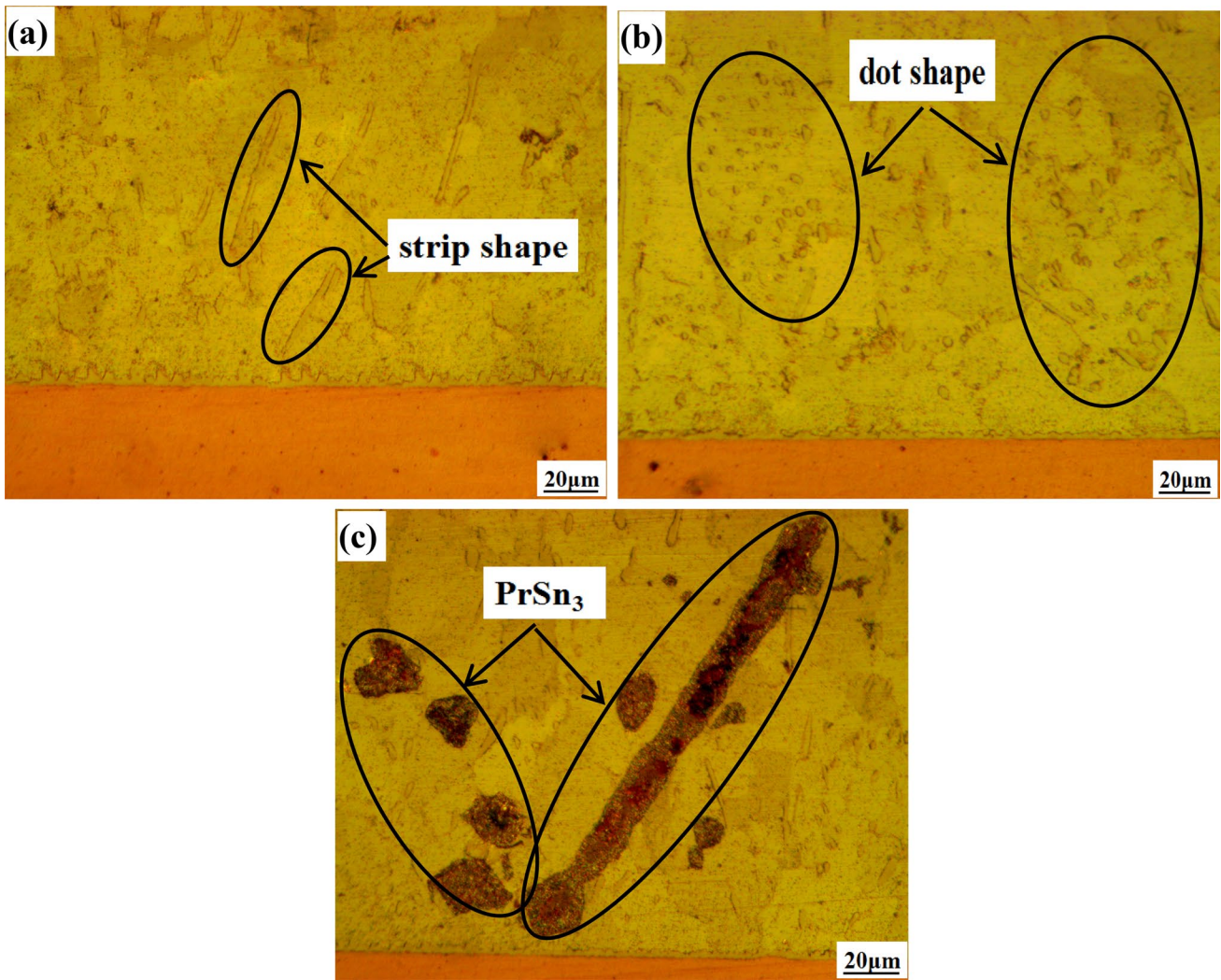

Fig. 11 Interfacial microstructures of Sn–0.3Ag–0.7Cu–xPr solder/Cu joints: **a** x = 0; **b** x = 0.06; **c** x = 0.5Pr
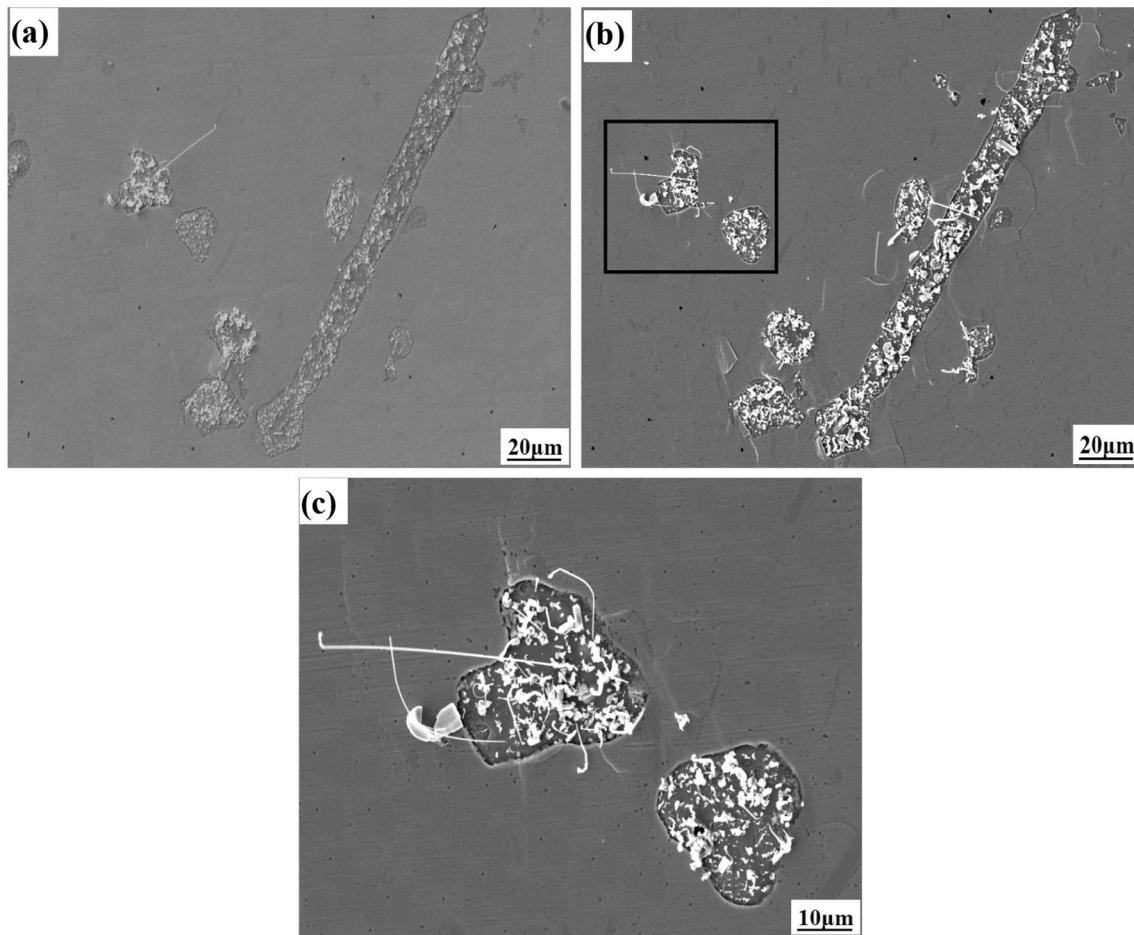
Fig. 12 SEM images of Sn whiskers on the surface of PrSn$_3$ shown in Fig. 11c at room temperature: **a** 1 day later, **b** 30 days later, **c** the enlarged SEM image of the selected area by *black rectangle* in **b**

solder matrix. Further, from the EDS analysis (Fig. 9b, c), it can be identified that the black phase contains elemental Sn and Pr and with an atom ratio of ~2.95. It should be mentioned that after trace amount of Pr addition, a formation of solid solution between Sn and Pr atoms is excluded since the difference in electronegativity (~0.83) is beyond the required range to form a solution (0.4) according to the Hume-Rothery criteria [25]. Besides, the radius difference between atoms of Sn and Pr (r_{Pr} = 18.3 Å; r_{Sn} = 14.1 Å) is about 23.0% that also exceeds the experimental range of radius difference to form solid solution (14–15%). Therefore, compounds will form after trace amount of Pr addition. Therefore, with assistance of Sn–Pr phase diagram, it was predicated to be PrSn$_3$. Besides, the strip-shaped IMC is ascertained to be Cu$_6$Sn$_5$ due to the Cu/Sn atom ratio in area B approaching to ~1.12. So, PrSn$_3$ was inclined to form at the interface of IMCs. Also, due to the appearance of elemental O, it can be obtained that this PrSn$_3$ has been oxidized (4 Pr Sn$_3$ + 3O$_2$ → 2Pr$_2$O$_3$ + 12Sn) just after

1 day at room temperature. It can be seen that some white dots also distributed on the surface of PrSn$_3$ and this was suggested to be the Sn whisker in the bud [6, 20, 26]. If this whisker bud has a further growth, it may cause circuit especially in high density electronic packages since it is conductive. Figure 10 gives the schematic illustration of the development and growth of Sn whisker. Clearly, it is the oxidation of PrSn$_3$ phase that not only provides sufficient Sn sources for the continuous formation and growth of Sn whiskers but also offers enough compressive stress for whisker buds to extrude out from the Pr$_2$O$_3$ oxidation layer. So, it can be assumed that once the oxidation of PrSn$_3$ phase finished, Sn whisker growth might stop due to the insufficient provision of both Sn sources and compressive stress. This assumption has been verified by in-situ observation of Sn whisker growth in the 0.5 wt% Pr-added solder joint, which was detailedly described in the following section.
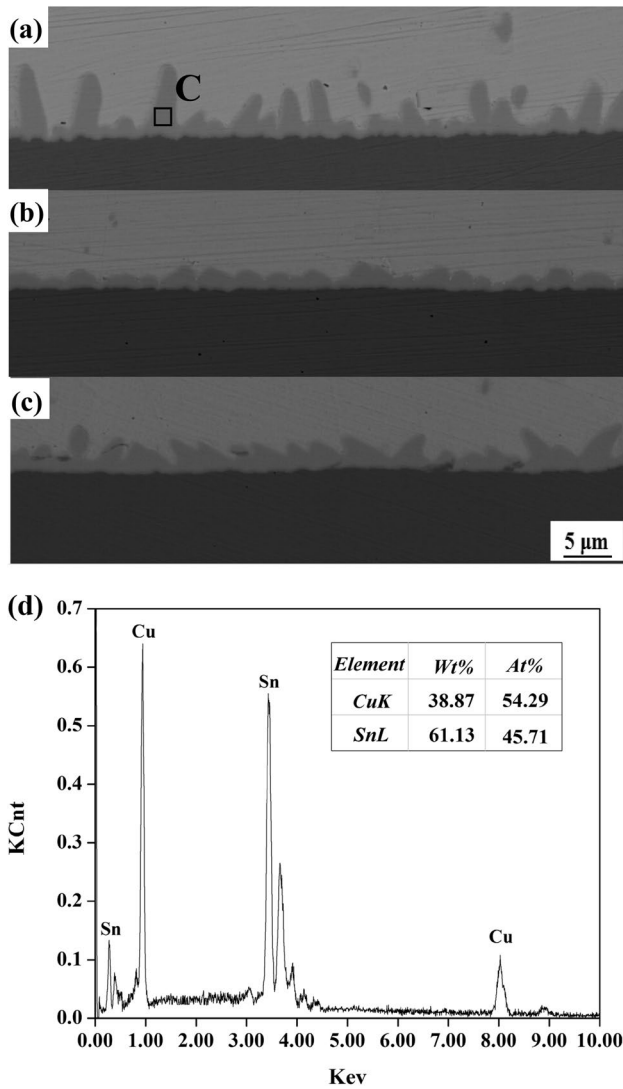
Fig. 13 Back scattered SEM micrographs of interfacial IMC layer of Sn–0.3Ag–0.7Cu–xPr/Cu solder joints: **a** x = 0; **b** x = 0.06; **c** x = 0.5; **d** EDS result of the area *C* in **a**

The effective refinement of the Sn–0.3Ag–0.7Cu solder matrix contributed by trace amount of Pr addition can be explained from three aspects. Firstly, RE Pr has a "Sn-affinity" characteristic that can reduce the activity of Sn atoms in the solder, which decreases the driving force for the primary IMC formation (e.g., Ag_3Sn, Cu_6Sn_5). Hence, IMCs with large size disappear. Secondly, the preferential formation of tiny Sn–Pr particles can serve as heterogeneous nucleation sites to accelerate the solidification process, thus leaving insufficient time for the growth of β-Sn or relative IMCs. Thirdly, since these tiny Sn–Pr particles are inclined to form at the grain interface of β-Sn dendrites or IMCs, they cause a pinning effect on grain boundary movement, which finally prevent the excessive growth of relative IMCs.

3.3.2 Microstructure at solder/Cu substrate interface

As is well-known, the mechanical property of solder joint is directly dependent on the interfacial microstructure of solder joint [4–6]. So, to fully understand how microstructure affects the mechanical properties of solder joint, three representative interficial microstructures of Sn–0.3Ag–0.7Cu–xPr/Cu solder joints (x = 0, 0.06 and 0.05 wt%) were selected to be studied, as shown in Fig. 11. Clearly, for the solder microstructure, with 0.06 wt%Pr addition, IMCs with strip shape in the original Sn-0.3Ag–0.7Cu solder changed into dot shape, which strengthened the solder matrix. The reason of this change of IMC shape has been introduced in last paragraph in Sect. 3.3.1. However, when 0.5 wt% Pr was added into the solder, large strip-shaped $PrSn_3$ appeared again. After 1 day at room temperature, obvious Sn whisker growth occurred, as shown in Fig. 12a. However, the morphology of Sn whiskers here exhibits some spindly and rod-shape besides the dot shape that formed in 0.5 wt% Pr-doped solder matrix (Fig. 9a). This may be related with the extra compressive stress provided by interfacial IMC growth, which makes the compressive stress around the oxidized $PrSn_3$ phase non-uniformly distribute. As a result, Sn whiskers grew at different rates and thereby exhibiting different morphology (spindly, cotton-like and short rod-like). After 30 days, an in-situ observation of the Sn whisker growth in the previous 0.5 wt% Pr-doped solder joint was made, as shown in Fig. 12b. Compared with Fig. 12a, it is clear that Sn whiskers grew further, but at a much slower rate. This can be proved by comparing the magnifying SEM image (Fig. 12c) of Sn whiskers in the selected area by black rectangle in Fig. 12b with those just after 1 day in Fig. 12a. As can be seen, Sn whiskers in Fig. 12c didn't have obvious growth after 30 days. This may be due to an decreased oxidation rate of $PrSn_3$ phase with time extending, which resulted in the insufficient supply of Sn sources and a reduction of compressive stress for Sn whisker growth.

It is well known that a thin, continuous and uniform IMC layer is an essential requirement for good bonding. But, a thick IMC layer might increase the brittleness of the interface, leading to easier crack initiation and propagation [7, 11]. Figure 13 shows the back scattered SEM micrographs of interfacial IMC layer of Sn–0.3Ag–0.7Cu–xPr/Cu solder joints (x = 0, 0.06 and 0.5). Clearly, all the joints exhibited a gray and continuous interfacial IMC layer. No defects, such as pinholes or microcracks, were observed at the interface between solders and substrates. For the Sn–0.3Ag–0.7Cu/Cu solder joint (Fig. 13a), the interfacial IMC layer with average thickness of ~5.01 μm exhibits a scallop-like shape. Small protruding portion marked with C near the solder interface, with the same color as the interfacial layer, was verified to be Cu_6Sn_5 by EDS analysis

Fig. 14 Schematic illustration of interfacial IMC growth of Sn–0.3Ag–0.7Cu–xPr solder joint: **a** x = 0; **b** x = 0.06 wt%; **c** x = 0.5 wt%
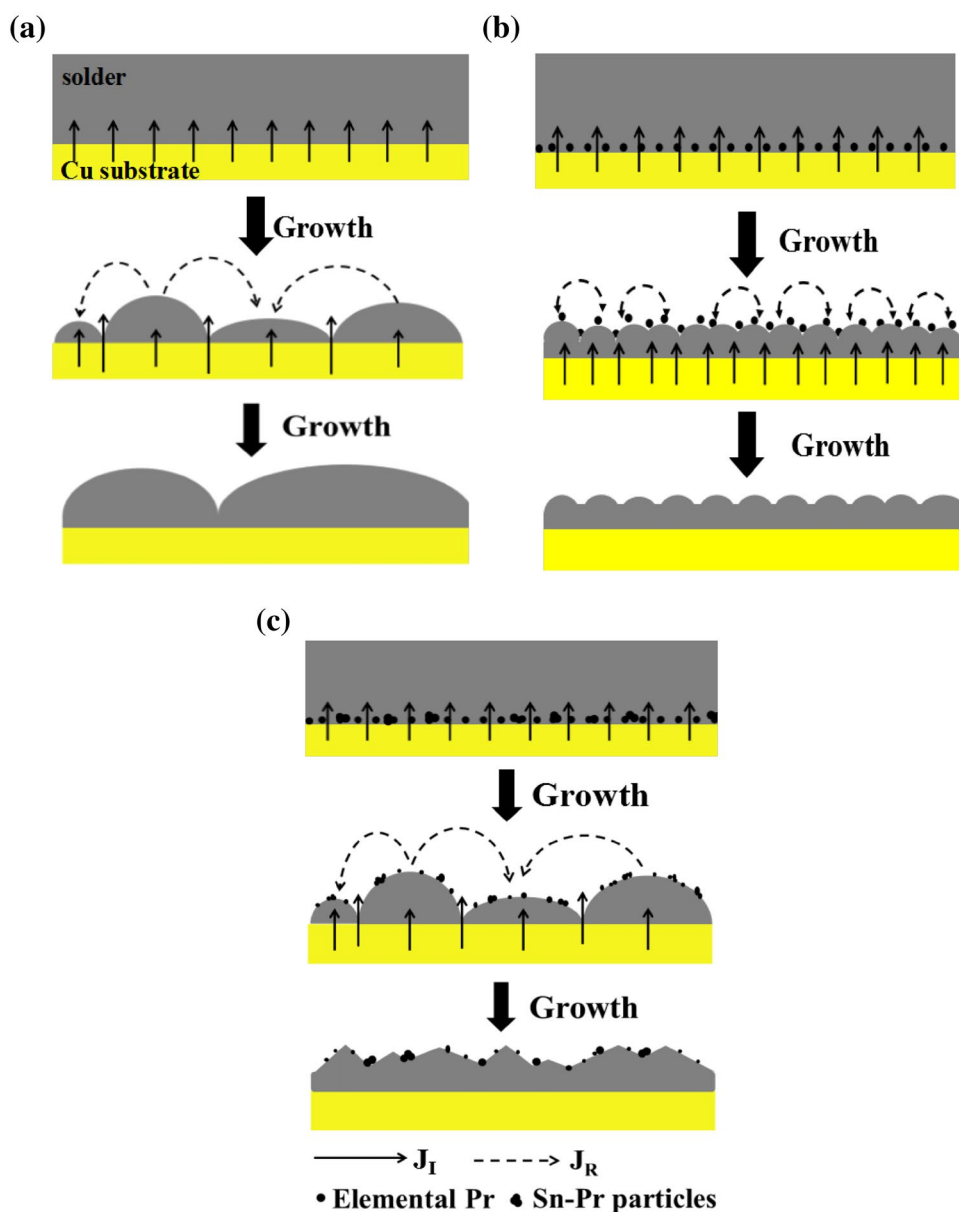
(Fig. 13d). Worthy of note is that due to the decrease in Ag content of the solder, there was no large plate-like Ag_3Sn IMCs at the interface that appeared in the Sn–3.8Ag–0.7Cu solder [8]. Therefore, no extra micro-cracks may occur at the interface when Sn–Ag–Cu low-Ag solder was applied in electronic packaging. After minor amount of Pr addition (0.06 wt%), the morphology of interfacial IMC layer became regular and relatively flat, as shown in Fig. 13b. Besides, the average thickness of the interfacial layer decreased to ~2.98 µm, which is about 40.5% thinner than that of Sn–0.3Ag–0.7Cu/Cu solder joint. Further, when increasing the Pr addition content to 0.5 wt%, the morphology was altered from regular and flat to prism-like and angular, which might easily induce micro-cracks at the interface. Moreover, the average thickness of IMC layer

in this moment have a little increase when compared with that of 0.06 wt% Pr-doped solder joint. Given the above, Sn–0.3Ag–0.7Cu–0.06Pr/Cu solder had the best mechanical property since it has a refined microstructure and a regular and relatively flat IMC layer with appropriate interfacial layer thickness. Meanwhile, it should be noted that excessive Pr addition may cause the formation of large $PrSn_3$ whose oxidation place may become the birthplace of Sn whiskers.

The alterations in morphology and thickness of interfacial IMC layer arising from different content of Pr addition can be explained by Fig. 14. It was suggested by Kim and Tu [27] that liquid channels, extending all the way to Cu_3Sn/Cu interface, existed between Cu_6Sn_5 scallops, which served as fast diffusion and dissolution paths for
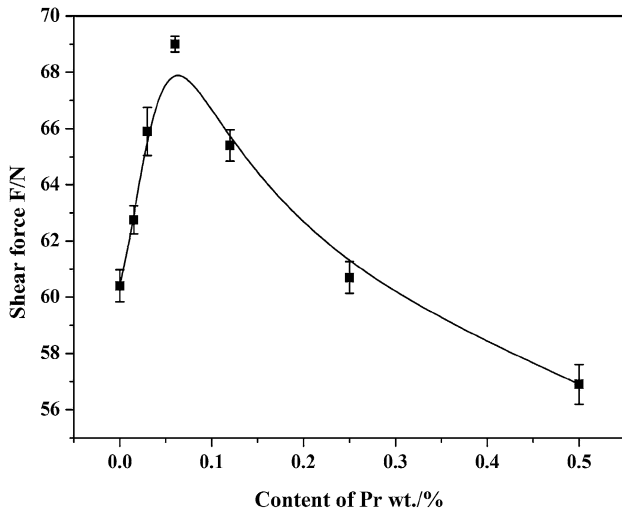
Fig. 15 Shear force of Sn–0.3Ag–0.7Cu–xPr (x = 0–0.5 wt%) solders

Table 2 Electronegativity differences between elemental Pr and Sn, Ag, Cu [28]

Element	Electronegativity	The difference value with Sn	The difference value with Ag	The difference value with Cu
Pr	1.13	0.83	0.8	0.77
Sn	1.96	0	0.03	0.06
Ag	1.93	0.03	0	0.03
Cu	1.90	0.06	0.03	0

Cu. Thus, the interfacial reaction was fed. Ignoring the appearance of Cu_3Sn IMC and other convenient chemical reactions, two kinds of fluxes were responsible for the scallop growth. One is ripening flux (J_R) and the other is interfacial reaction flux (J_I), as shown in Fig. 14a. As can be seen, flux (J_R) is responsible for the coalescence of Cu_6Sn_5 scallops and increment in diameters, while flux (J_I) feeds the thickness growth of IMC layer. At the beginning of reaction, Cu_6Sn_5 scallops nucleate at the solder/substrate interface induced by the concentration gradient between solder and Cu substrate [5]. The scallops grow with time extending as Cu is supplied by the flux (J_R) and (J_I). However, when 0.06 wt% Pr was added into the solder, they will uniformly adsorb on the surface of Cu substrate, as shown in Fig. 14b. Hence, the movement of Cu atoms from substrate to liquid solder is hindered and a reduction in flux (J_I) is obtained, which help reduce the thickness of IMC layer. With further reaction, the coalescence of neighboring scallops is also impeded, which finally decreases flux (J_R) and reduces the scallop diameter. Correspondingly, not only the thickness of IMC layer is reduced, but also its morphology becomes much

more flat and regular in comparison to that at the no-added Sn–0.3Ag–0.7Cu/Cu interface. However, when the content of Pr approaches to 0.5 wt%, part of small Sn–Pr particles grow attached to the Cu substrate, as shown in Fig. 14c. There exists a different extent of effect on the interfacial reaction between the grown Sn–Pr particles and elemental Pr. Therefore, the interfacial reaction flux (J_I) might be decreased to different degree and with further growth, the ripening (J_R) flux will also be affected to different level. As a result, the morphology of IMC layer will change from regular and flat to prism-like and angular.

3.4 Shear force and fracture behavior of solder joint

In microelectronic packaging, solder joint usually provides both electrical and mechanical support, making studying mechanical property of solder joint particularly essential [16, 19]. Figure 15 shows the effect of Pr addition on the shear force of Sn–0.3Ag–0.7Cu/Cu solder joint. It can be seen that as the content of Pr addition increased, the shear force of solder joint first increased to the maximum value of 69.1 N, and then rapidly decreased. This maximum shear force was achieved by 0.06 wt% Pr-modified solder joint, which is 14.2% higher than its monolithic counterpart. This enhancement in shear force contributed by minor amount of Pr addition can be explained as follows. Sn–Pr particles will preferentially nucleate than any other binary groups that are possible to yield over solidification since the differences in electronegativity between elemental Pr and Sn is the greatest among all the binary groups, as shown in Table 2 [28]. These tiny Sn–Pr particles will pin the linear dislocations, increase dislocation densities, restrict grain boundary motions and finally strengthen the solder matrix. However, a further Pr addition caused a sharp decrease in the shear force of the corresponding solder, which is related to the oxidation of Sn–Pr phase. Therefore, it's necessary to manage the content of Pr addition well to maximize the refinement effect on microstructure and to prevent the appearance of Sn whisker. In combination with the experimental results shown above, the most suitable content of Pr addition is about 0.06 wt%.

Figure 16 shows the SEM micrographs of fracture surfaces of Sn–0.3Ag–0.7Cu–xPr (x = 0, 0.06, 0.5 wt%) solder joints after shear force test. Apparently, the fracture surface of solder joint was parallel to the shear loading direction. As shown in Fig. 16a, b, dimple-like structures appeared on the fracture surfaces of both Sn–0.3Ag–0.7Cu/Cu and Sn–0.3Ag–0.7Cu–0.06Pr/Cu solder joint, which indicates a ductile fracture with micro-void nucleation and coalescence mechanism of failure. Worthy of note is that the size of dimple on the fracture surface of 0.06Pr-doped solder joint was much smaller than that of the non-added solder

joint. This indicates that the ductility of Sn–0.3Ag–0.7Cu solder can be improved by an optimal amount of Pr addition. In addition, IMC particles (marked with D in Fig. 16a) existing at the bottom of the dimples, which serve as void-nucleation sites, were ascertained to be Cu_6Sn_5 by EDS analysis, as shown in Fig. 16d. However, for the fracture

surface of Sn–0.3Ag–0.7Cu–0.5Pr solder joint (Fig. 16c), various sizes of dimples can be seen due to non-uniformly distributed IMC particles. Besides, the area of dimples decreased and there appeared some river line patterns, which indicates that after excessive Pr addition, the failure mode of solder joint transformed from ductile fracture into
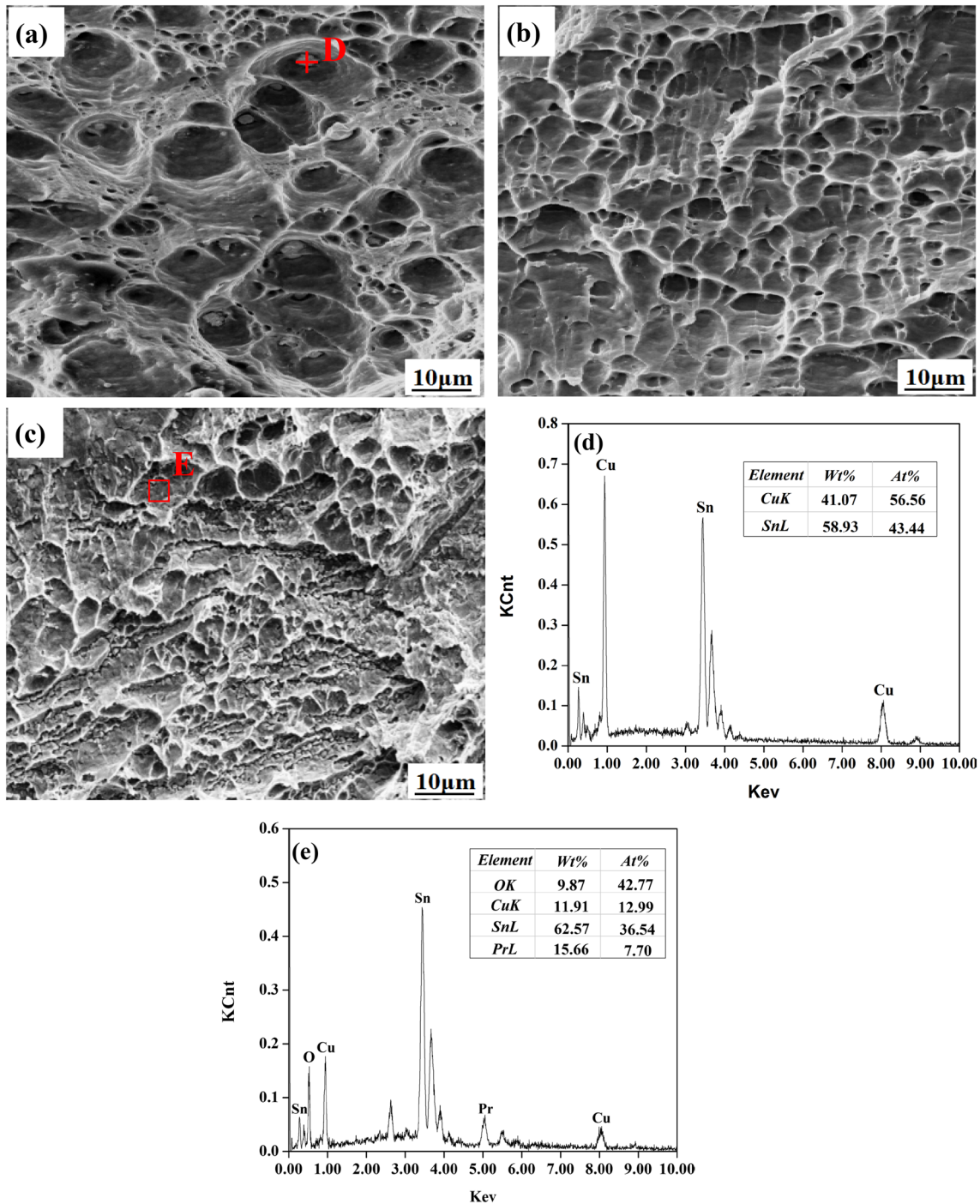

Fig. 16 Fracture morphologies of Sn–0.3Ag–0.7Cu–xPr after shear test: **a** x = 0; **b** x = 0.06; **c** x = 0.5 wt%; **d** EDS analyzed result of point *D* in **a**; **e** EDS analyzed result of point *E* in (**c**)

cleavage fracture. Moreover, the area marked E in Fig. 16c was analyzed by EDS and the results shown in Fig. 16e indicated that some oxidized Sn–Pr phases might exist in this area. So, the change in the morphology of fracture surface after Pr addition indicates again that optimal Pr addition (0.06 wt%) can enhance the mechanical properties of the solder joint.

4 Conclusions

In this study, the evolution of microstructure and properties of Sn–0.3Ag–0.7Cu–xPr low-Ag solders (x = 0–0.5 wt%) for electronic applications was investigated. From the experimental results above, the following conclusions can be drawn:

(1) The wettability of Sn–0.3Ag–0.7Cu solder would be evidently improved by optimal amount of Pr addition and this amount is about 0.06 wt%. Also, elevating the soldering temperature to a proper extent can better the wetting performance of solders.

(2) Trace amount of Pr addition refined the (interfacial) microstructure of solder and with the maximum refinement realized for solder containing 0.06 wt% Pr. Meanwhile, in this moment, the thickness of its interfacial IMC layer decreased to ~2.98 μm, which is about 40.5% thinner than that of non-modified solder joint. Besides, the morphology of interfacial IMC layer also became regular and relatively flat. We have explained the change of morphology and thickness of interfacial IMC layer after Pr addition based on the Kim and Tu's kinetic model of interfacial IMC growth.

(3) With 0.06 wt% Pr addition, both shear force and ductility of solder joint also had an obvious enhancement. However, excessive Pr addition was harmful to the shear force of solder joint due to the formation of hard and brittle oxidized $PrSn_3$ phase. Besides, with Pr addition from 0 to 0.5 wt%, the fracture mode of solder joint also gradually changed from ductile fracture to cleavage fracture. So, it is important to manage the content of Pr addition well or partial amount of Pr addition may lose its effectiveness and some bad effects on properties might appear.

(4) When excessive content of Pr was added into the solder, black and fish-bone shaped $PrSn_3$ phase appeared, which were easy to be oxidized and became the birthplace of Sn whiskers. By in-situ observation of Sn whisker growth in 0.5 wt% Pr-doped solder joint, it can be obtained that the incubation period of Sn whisker is short. However, with time extending its growth rate may have a great decrease. Meanwhile, it was found after 1 day at room temperature, spindly and rod-like Sn whiskers also grew in 0.5 wt% Pr-doped solder joint besides dot-shaped Sn whisker that grew in 0.5 wt% Pr-doped solder matrix. We suggest this may be related with the extra compressive stress provided by interfacial IMC layer growth in 0.5 wt% Pr-doped solder joint.

References

1. H.Q. Wang, H. Zhao, D.P. Sekulic, Y.Y. Qian, A comparative study of reactive wetting of lead and lead-free solders on Cu and (Cu_6Sn_5/Cu_3Sn)/Cu substrates. J. Electron. Mater. **37**(10), 1640–1647 (2008)
2. J.C. Xu, et al., Study on microstructure and properties of Sn-0.3Ag-0.7Cu solder bearing Nd. J. Mater. Sci. (2016). doi:10.1007/s10854-016-4901-y
3. J. Wang, H.M. Wei, P. He, T.S. Lin, F.J. Lu, Microstructure and mechanical properties of tin-bismuth solder reinforced by aluminum borate whiskers. J. Electron. Mater. **44**(10), 3872–3879 (2015)
4. L. L. Gao, et al., Effects of trace rare earth Nd addition on microstructure and properties of SnAgCu solder. J. Mater. Sci. **21**(7), 643–648 (2010)
5. L. Zhang et al., Properties enhancement of SnAgCu solders containing rare earth Yb. Mater. Des **57**, 646–651 (2014)
6. G. Zeng et al., Interfacial microstructure and properties of Sn–0.7Cu–0.05 Ni/Cu solder joint with rare earth Nd addition. J. Alloy. Compd. **509**(25), 7152–7161 (2011)
7. K.S. Kim, S.H. Huh, K. Suganuma, Effects of intermetallic compounds on properties of Sn–Ag–Cu lead-free soldered joints. J. Alloy. Compd. **352**(1), 226–236 (2003)
8. L. L. Gao, et al., Effect of praseodymium on the microstructure and properties of Sn3.8Ag0.7Cu solder. J. Mater. Sci. **21**(9), 910–916 (2010)
9. M. Osterman, M. Pecht, Strain range fatigue life assessment of lead-free solder interconnects subject to temperature cycle loading. Solder. Surf. Mt. Technol. **19**(2), 12–17 (2007)
10. A.A. El-Daly et al., Influence of Zn addition on the microstructure, melt properties and creep behavior of low Ag-content Sn-Ag-Cu lead-free solders. Mater. Sci. Eng. A **608**, 130–138 (2014)
11. D. X. Luo, S. B. Xue, S. Liu, Investigation on the intermetallic compound layer growth of Sn-0.5Ag-0.7Cu-xGa/Cu solder joints during isothermal aging. J. Mater. Sci. **25**(12), 5195–5200 (2014)
12. K. Kanlayasiri, M. Mongkolwongrojn, T. Ariga, Influence of indium addition on characteristics of Sn-0.3Ag-0.7 Cu solder alloy. J. Alloy. Compd. **485**(1), 225–230 (2009)
13. A.A. El-Daly et al., Microstructure, mechanical properties, and deformation behavior of Sn-1.0 Ag-0.5 Cu solder after Ni and Sb additions. Mater. Des. **43**, 40–49 (2013)
14. L.C. Tsao et al., Influence of TiO_2 nanoparticles addition on the microstructural and mechanical properties of Sn0.7Cu nano-composite solder. Mater. Sci. Eng. A **545**, 194–200 (2012)
15. A.A. El-Daly et al., Novel SiC nanoparticles-containing Sn-1.0Ag-0.5 Cu solder with good drop impact performance. Mater. Sci. Eng. A **578**, 62–71 (2013)

16. L. Zhang, K. N. Tu, Structure and properties of lead-free solders bearing micro and nano particles. Mater. Sci. Eng. **82**, 1–32 (2014)
17. H.T. Lee et al., Effect of La addition on adhesive strength and fracture behavior of Sn-3.5Ag solder joints. Mater. Sci. Eng. A **528**(10), 3630–3638 (2011)
18. L. Zhang et al., Microstructure characterization of SnAgCu solder bearing Ce for electronic packaging. Microelectron. Eng. **88**(9), 2848–2851 (2011)
19. L. Zhang, et al., Properties and microstructures of SnAgCu-xEu alloys for concentrator silicon solar cells solder layer. Sol. Energy Mat. Sol. C **130**, 397–400 (2014)
20. T. H. Chuang, Rapid whisker growth on the surface of Sn-3Ag-0.5 Cu-1.0 Ce solder joints. Scripta. Mater. **55**(11), 983–986 (2006)
21. Japanese Industrial Standards Committee, JIS Z 3198-4: 2003. Test Methods For Lead-Free Solders—Part 4: Methods for Wettability Test by a Wetting Balance Method and a Contact Angle Method (2003)
22. Japanese Industrial Standards Committee, JIS Z 3198-7: 2003. Test Methods For Lead-Free Solders—Part 7: Methods For Shear Test Of Solder Joints On Chip Components (2003)
23. Solderability Tests for Component Leads, Terminations, Lugs, Terminals and Wires, IPC/EIA/JEDEC J-STD-003B, 2003
24. X. J. Liu, et al., Thermodynamic Calculation of phase equilibria in the Sn-Ag-Cu-Ni-Au System. J. Electron. Mater. **36**(11), 1429–1441 (2007)
25. W. Humerothery, G. V. Raynor, Book Reviews: The Structure of Metals and Alloys. Science **120**, 1–383 (1954)
26. M.A. Dudek, N. Chawla, Mechanisms for Sn whisker growth in rare earth-containing Pb-free solders. Acta Mater. **57**(15), 4588–4599 (2009)
27. H.K. Kim, T.N. Tu, Kinetic analysis of the soldering reaction between eutectic SnPb alloy and Cu accompanied by ripening. Phys. Rev. B **53**(23), 16027–16034 (1996)
28. R.L. DeKock, H.B. Gray, *Chemical structure and bonding* (University Science Books, Sausalito, 1989), p. 91